New insight in the uranium valence state determination in UyNd1-yO2-x

Bes, R.; Kvashnina, K.; Rossberg, A.; Dotavio, G.; Desgranges, L.; Pontillon, Y.; Solari, P. L.; Butorin, S. M.; Martin, P.;

Originally published:

May 2018

Journal of Nuclear Materials 507(2018), 145-150

DOI: https://doi.org/10.1016/j.jnucmat.2018.04.046

Perma-Link to Publication Repository of HZDR:

https://www.hzdr.de/publications/Publ-26177

New insight in the uranium valence state determination in $U_yNd_{1-y}O_{2\pm x}$

R. Bès[a,*], K. Kvashnina[b,c], A. Rossberg[b,c], G. Dotavio[d], L. Desgranges[d], Y. Pontillon[e], P.L. Solari[f], S.M. Butorin[g], P. Martin[h]

[a]*Department of Applied Physics, Aalto University, P.O. Box 14100, FI-00076 Aalto, Finland*
[b]*Rossendorf Beamline at ESRF - The European Synchrotron, CS40220, 38043 Grenoble Cedex 9, France*
[c]*Helmholtz Zentrum Dresden-Rossendorf (HZDR), Institute of Resource Ecology, P.O. Box 510119, 01314 Dresden, Germany*
[d]*CEA, DEN, DEC, F-13108 Saint Paul Lez Durance Cedex, France*
[e]*CEA/DEN/CAD/DEC/SA3C/LAMIR, Saint Paul lez Durance, France*
[f]*Synchrotron SOLEIL, Ligne de Lumière MARS, L'Orme des Merisiers, Saint Aubin, BP 48, F-91192 Gif-sur-Yvette Cedex, France*
[g]*Molecular and Condensed Matter Physics, Department of Physics and Astronomy, Uppsala University, P.O. Box 516, SE-751 20 Uppsala, Sweden.*
[h]*CEA, Nuclear Energy Division, Research Department on Mining and Fuel Recycling Process, SFMA/LCC, Bagnols-sur-Cèze, France*

Abstract

The charge compensation mechanisms in $U_yNd_{1-y}O_{2\pm x}$ and its consequence on the overall O stoichiometry (or O/M ratio where M=Nd+U) have been studied through the uranium valence state mixture evolution as a function of Nd content up to y=0.62 by means of high energy resolution fluorescence detection X-ray absorption spectroscopy (HERFD-XAS) at the U M_4-edge. Our results clearly demonstrate the formation of U^{5+} at low Nd content ($y < 0.15$). Upon increasing the Nd content, oxygen vacancies and the formation of U^{6+} appear as competing mechanisms for intermediate Nd concentrations, leading to the co-existence of $U^{4+}/U^{5+}/U^{6+}$ mixed valence and an overall hypostoichiometry ($O/M < 2.00$). Finally, the formation of U^{6+} associated with strongly distorted U local environment

*Corresponding author
Email addresses: rene.bes@aalto.fi (R. Bès)

is observed for high Nd concentrations (y=0.62), leading to an overall hyperstoichiometry (O/M < 2.00).

---

1. Introduction

Since many decades, uranium oxide UO_2 is used as fuel in nuclear power plants. Among the non volatile fission products created during in-pile irradiation, the lanthanides (Ln) represents approximately 35 weight % of the inventory [1]. These elements are known to be soluble into the UO_2 structure and to form a solid solution over a wide range of composition (U,Ln)$O_{2\pm x}$ [2], but lattice parameters change depends of the irradiation conditions [3–6]. The existence of such solid solution is expected to be correlated to uranium valence states flexibility (from U^{4+} to U^{5+} and U^{6+}) and to the formation of oxygen vacancies, which both ensure the charge neutrality [7]. Nevertheless, recent studies have demonstrated the existence of a miscibility gap at room temperature for samples containing higher than 3 at. % of Nd [8–10]. In these studies, high temperature X-ray Diffraction (XRD) measurements as well as Raman spectroscopy have highlighted the coexistence of two Face Centered Cubic (FCC) phases exhibiting different oxygen stoichiometry or O/M ratio (M=U+Nd) leading to the general formula $U_yNd_{1-y}O_{2\pm x}$ and $U_yNd_{1-y}O_{2.00}$. The miscibility gap appears to be stable up to 745-800 K [9]. For higher temperatures, only one $U_yNd_{1-y}O_{2-x}$ phase is present. In $U_yPu_{1-y}O_{2-x}$ [11] and $U_yCe_{1-y}O_{2-x}$ [12] systems, a miscibility gap also exists for y > 0.2, with the coexistence of oxygen vacancy and uranium valence states U^{5+} for an overall hypostoichiometric formula (O/M < 2). However, such coexistence in $U_yNd_{1-y}O_{2\pm x}$ remains an open question as no clear experimental evidence is reported in literature.

X-ray absorption spectroscopy (XAS) is particularly advantageous to probe

electronic and local structure of actinide materials, by means of X-ray absorption near edge structure (XANES) and extended X-ray absorption fine structure (EXAFS). In addition, the penetrating nature of X-rays in the 3-20 keV energy range, i.e. actinide's $M_{4,5}$- and L_3-edges, allows to analyze confined samples, avoiding risks of radionuclei dispersion, and the use of synchrotron radiation limits the masses of the samples that are investigated [13]. But, considering the broadening of XANES spectra due to core-hole, the observation of very fine details can be limited. Moreover, the most used U L_3-edge XANES can also be strongly affected by the local geometry [14, 15]. One major difficulty is often the unavailability of reference compounds with both the correct symmetry and the same valence. However, linear combination fitting of U L_3-edge XANES spectra gives accurate results for mixed actinides such (U,Am)O_2 and (U,Pu)O_2 in deducing the overall actinides valence and the oxygen stoichiometry of the samples [16–21]. In the case of oxides without a stable fluorite structure at room temperature such as trivalent lanthanides, incorrect intensities deduced by linear combination fitting would subsequently lead to incorrect evaluation of the uranium valence state mixture. Thanks to the recent development of X-ray emission spectrometer, one can directly probe the 5f and 6d electron density of states and local structure with a virtually reduced core-hole lifetime broadening. This approach, high energy resolution fluorescence detected-XAS (HERFD-XAS), allows highly precise electronic and local structure of actinides, including direct evaluation of valence state mixture [22]. For example, this approach has been successfully applied to (U,Bi)O_2 mixed oxides [23].

By taking advantage of the HERFD-XAS capability, this paper aims to provide accurate U valence state's evaluation on $U_yNd_{1-y}O_{2\pm x}$ samples as a function of Nd content. Such key knowledge would give important insights about O/M ratio behavior and is here discussed through electroneutrality and the associated charge compensation mechanisms.

2. Material and experimental methods

2.1. Sample preparation

The $U_yNd_{1-y}O_{2\pm x}$ samples were prepared by homogeneously mixing Nd_2O_3 and UO_2 powders with targeted Nd/(U+Nd) ratios. The sample compositions are given in Table 1. The powders were pressed at 450 MPa and sintered during 72 hours in a reductive atmosphere (dry Ar + 5% H_2) at 1973 K. Subsequent room temperature X-ray Diffraction characterization showed that final pellets are free of Nd_2O_3 precipitates [8]. In order to limit oxidation/hydration process during sample storage, the pellets were confined between two glued 12.5 μm kapton foils.

2.2. X-ray absorption spectroscopy

The U L_3-edge XANES measurements were carried out at the MARS beamline [24] located at the French synchrotron radiation facility SOLEIL (France). The photon energy was scanned from 17100 to 17300 eV, using the Si(220) sagittal focusing double-crystal monochromator (DCM). Rejection of higher harmonics as well as vertical collimation/focusing was achieved by two platinum-coated mirrors, placed before and after the DCM, working under total reflection at 3.1 mrad. The beam size was estimated to be about 0.3 mm both vertically and horizontally. Energy calibration was achieved using the first infection point of XANES spectra collected at Y K-edge of an yttrium (17038 eV) metallic foil. The XANES spectra were collected in fluorescence mode at room temperature using a Vortex-90-EX silicon drift detector (SDD). The total energy resolution is estimated to be about 8.3 eV.

The U M_4-edge XANES measurements were performed at the ID26 beamline [25] of the European synchrotron-ESRF (France). The U M_4-edge incident energy (3725 eV) was selected using the Si(111) double crystal monochromator.

Three Si mirrors at 3.5 mrad working under total reflection achieved rejection of higher harmonics. The beam size was estimated to be about 0.2 mm vertically and 0.4 mm horizontally. HERFD-XANES spectra were measured using a X-ray emission spectrometer equipped with five Si(220) crystal analysers and a silicon drift diode in a vertical Rowland geometry. The spectrometer was tuned to the maximum of the U M_β ($3d_{3/2}$-$4f_{5/2}$, 3337 eV) X-ray emission line using the (220) reflection of the Si analyser crystals at a Bragg angle of 75.4°. The detected intensity was normalized to the incident flux. A combined (incident convoluted to emitted) energy resolution of 0.4 eV was obtained as determined by measuring the full width at half maximum (FWHM) of the elastic scattering peak.

The experiments reported here were performed at room temperature in air without any additional environment around the sample. The paths of the incident and emitted X-rays through air during the experiments were minimized in order to avoid losses in intensity due to absorption in the air.

The ATHENA software [26] was used for normalizing XANES spectra from the raw absorption data. Pre-edge removal and normalization were achieved using linear functions at the U L_3-edge. U M_4-edge spectra were normalized with respect to their maximum. The energy threshold (E_0) values and the white-line maximum energy values of each spectrum were chosen respectively as the first inflection point and the first knot of the first derivative relatively to the incident energy.

The iterative target test (ITT) associated to the Principal Component Analysis (PCA) as available within the ITFA code [27] has been used in order to extract the uranium valence relative concentration (U^{4+}, U^{5+} and U^{6+}) from HERFD spectra. Three components were then considered and spectra collected on UO_2, $NaUO_3$ and β-UO_3 were used as pure components for U^{4+}, U^{5+} and U^{6+} respectively. The value of these component has been fixed to 100 % and/or 0 % in the case of the 3 pure valence reference samples. They were left free for the $U_yNd_{1-y}O_{2\pm x}$ samples.

3. Experimental results and discussion

The uranium L_3-edge XANES spectra of $U_yNd_{1-y}O_{2\pm x}$ samples are reported in Figure 1.

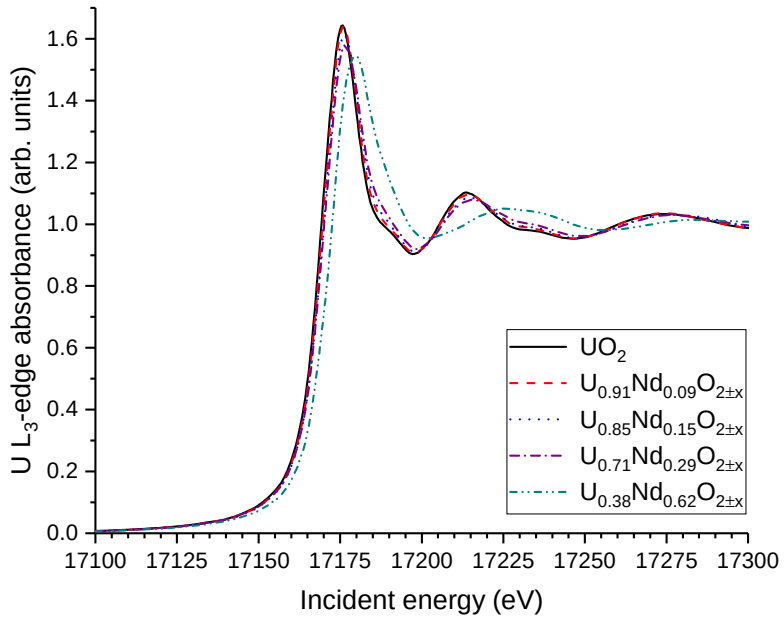

Figure 1: Uranium L_3-edge XANES experimental spectra recorded on UO_2 and $U_yNd_{1-y}O_{2\pm x}$ samples as collected on MARS.

The UO_2 XANES spectrum consists of an intense peak, so-called the white-line and situated at 17175.0(5) eV, and on additional resonance, at a higher energy, around 17212.9(5) eV. A shoulder on the right side of the white line is also observed at 17188.3(5) eV. The inflection point, E_0, was found at 17169.0(5) eV. The corresponding values for the Nd doped samples are reported in Table 1.

Except for the $U_{0.38}Nd_{0.62}O_{2\pm x}$ sample, all the Nd doped UO_2 samples show spectral features close to the UO_2 one. The uranium local environment is clearly

Table 1: Energy position of the main spectral features observed in the U L_3-edge spectra.

Sample	E_0 (eV)	White-line (eV)	Shoulder (eV)	Resonance (eV)
UO_2	17169.0(5)	17175.0(5)	17188.3(5)	17212.9(5)
$U_{0.91}Nd_{0.09}O_{2\pm x}$	17169.7(5)	17175.3(5)	17188.5(5)	17213.6(5)
$U_{0.85}Nd_{0.15}O_{2\pm x}$	17169.9(5)	17175.4(5)	17188.6(5)	17213.5(5)
$U_{0.71}Nd_{0.29}O_{2\pm x}$	17170.0(5)	17175.9(5)	17188.4(5)	17214.5(5)
$U_{0.38}Nd_{0.62}O_{2\pm x}$	17172.8(5)	17179.0(5)	-	17224.8(5)

maintained in the uranium rich region up to y=0.29. A slight shift toward high energy is observed for E_0. In addition, the white-line intensity decreases and the shoulder intensity increases simultaneously upon increasing the Nd content. A similar behavior was observed in $U_{1-y}Gd_yO_2$ [28] and in $U_{1-y}Am_yO_2$ [18, 19, 21] samples where Am was purely trivalent. It is attributed to the formation of U^{5+} as charge compensation mechanism in both $U_{1-y}Gd_yO_2$ and $U_{1-y}Am_yO_2$.

Strong changes in uranium local environment have to be expected in the Nd rich region. Indeed, the overall shape of the $U_{0.38}Nd_{0.62}O_{2\pm x}$ spectrum is quite different from the UO_2 one. Moreover, a chemical shift of about 3.8 eV is observed for E_0, giving insights on the absence of U^{4+} in that sample. But, as previously explained, the U L_3-edge is strongly affected by the local geometry around U atoms in reference compounds leading to the informal rule: the closer the local environment is, the most accurate the valence state ratios are. But, no face centered cubic phases are reported with pure U^{5+} and U^{6+} valence states. For U $M_{4,5}$-edge HERFD-XANES spectra, chemical shifts are better resolved than for U L_3-edge and spectra shows similar shapes for different local environments [22, 29, 30]. So, U $M_{4,5}$-edge appears to be the best choice in that case.

The uranium M_4-edge HERFD-XANES spectra of $U_{1-y}Nd_yO_{2\pm x}$ samples are

reported in Figure 2. They are compared to the reference spectra of UO_2, $NaUO_3$ and β-UO_3. These stoichiometric and single-phase reference compounds correspond to pure U^{4+}, U^{5+} and U^{6+} valence state respectively.

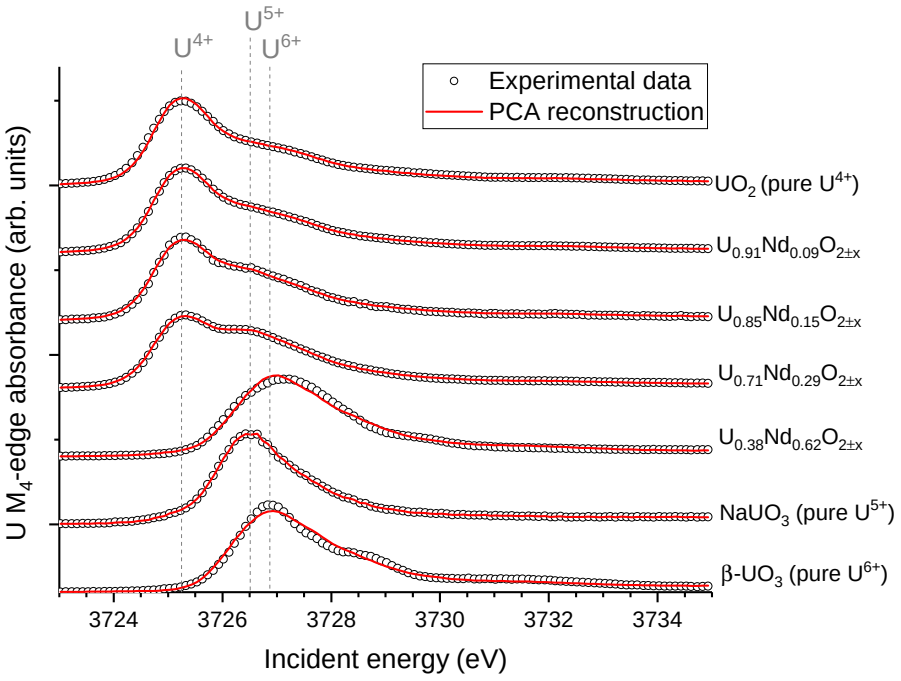

Figure 2: Uranium M_4-edge HERFD-XANES experimental spectra (dots) recorded on UO_2, $NaUO_3$, β-UO_3 and $U_yNd_{1-y}O_{2\pm x}$ collected on ID26. The X-ray emission spectrometer was tuned to the maximum energy of the M_β emission line. The reconstructed spectra (from PCA) are given (full lines) for each spectrum.

As expected, all the Nd doped UO_2 samples, excepting $U_{0.38}Nd_{0.62}O_{2\pm x}$, show spectral features close to the UO_2 one, confirming the previous conclusions at U L_3-edge, but the U^{5+}/U^{6+} contributions are here more clearly identified. The corresponding spectral feature energy positions are reported in Table 2.

The increasing intensity of the shoulder at the right side of the U^{4+} white-

Table 2: Overview and comparison to literature data of incident energy at the white-line position for the studied samples as indicated in Figure 2.

Sample	White-line (eV)			Reference
	U^{4+}	U^{5+}	U^{6+}	
UO_2	3725.3(2)	-	-	This work
UO_2	3725.5(2)	-	-	[30]
$NaUO_3$	-	3726.6(2)	-	This work
KUO_3	-	3726.4(2)	-	[30]
β-UO_3	-	-	3726.9(2)	This work
β-UO_3	-	-	3726.8(2)	[30]
$U_{0.91}Nd_{0.09}O_{2\pm x}$	3725.3(2)	3726.6(2)	-	This work
$U_{0.85}Nd_{0.15}O_{2\pm x}$	3725.3(2)	3726.5(2)	-	This work
$U_{0.71}Nd_{0.29}O_{2\pm x}$	3725.3(2)	3726.5(2)	-	This work
$U_{0.38}Nd_{0.62}O_{2\pm x}$	-	-	3727.1(2)	This work

line indicates the formation of U^{5+} and/or U^{6+} valence state [22, 29, 30]. The $U_{0.38}Nd_{0.62}O_{2\pm x}$ sample does not show any U^{4+} feature and is most probably composed by a mixture of U^{5+} and U^{6+} only, even if its spectrum is dominated by U^{6+} white-line. The PCA reconstructed spectra are shown in Figure 2. An overall agreement between the experimental spectra and the reconstructed spectra using the three principal components is obtained, except for the Nd rich sample and β-UO_3. This is probably the consequence of very different local symmetry around U one can expect comparing $NaUO_3$, β-UO_3 and the bixbyite-like structure expected for very high Nd content. However, the fitting result confirms that U^{6+} valence states is predominant in that case. The deduced valence concentrations $[U^{4+}]$, $[U^{5+}]$ and $[U^{6+}]$ are drawn as a function of the Nd content in Figure 3 and are reported in Table 3.

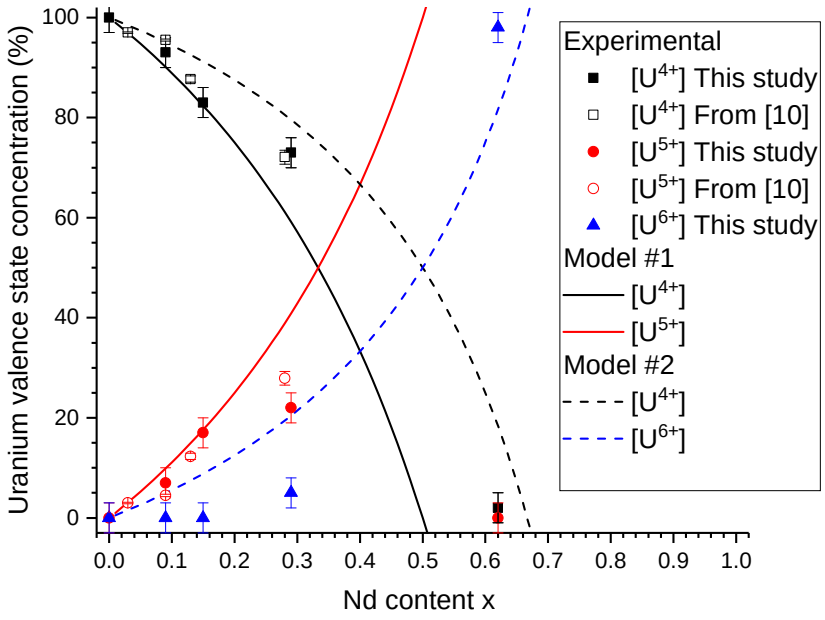

Figure 3: Uranium valence state relative concentrations deduced from Principal Component Analysis (full symbols) and their expected evolution (full lines) according to two different models of charge compensation mechanism. The values published by Dottavio et al. [10] deduced from X-ray Diffraction with subsequent Rietveld refinement (empty symbols) are also shown for comparison.

One can see that in the U-rich region, there is no U^{6+}, but only U^{5+}. In the Nd-rich region, both U^{5+} and U^{5+} are formed, and U^{4+} is no more observed.
In Figure 3, the measured uranium valence states' concentration are compared with two different compensation models in order to understand the underlying mechanisms involved in the charge compensation when adding a trivalent atoms in UO_2. The first model, called Model #1, corresponds to the formation of U^{5+}. The second one, called Model #2, is the formation of U^{6+}. Both models keep stoichiometry, with no deviation from O/M=2.00 as $[U^{6+}]=[Nd^{3+}]$ and $[U^{6+}]=2*[Nd^{3+}]$. An

Table 3: Valence concentrations [U4+], [U5+] and [U6+] in % of U as deduced from PCA analysis. Uncertainty are about 3%.

Sample	$[U^{4+}]$	$[U^{5+}]$	$[U^{6+}]$
$U_{0.91}Nd_{0.09}O_{2\pm x}$	93%	7%	0%
$U_{0.85}Nd_{0.15}O_{2\pm x}$	83%	17%	0%
$U_{0.71}Nd_{0.29}O_{2\pm x}$	73%	22%	5%
$U_{0.38}Nd_{0.62}O_{2\pm x}$	2%	0%	98%

additional compensation mechanism would be the formation of oxygen vacancies V_O, and is called Model #3. This model leads to no change in the uranium valence concentration and so does not appear in Figure 3. However, Model #3 directly affects the global O/M ratio by reducing the oxygen content by y/2 and leads to an overall hypostoichiometry, that could be associated to the reported miscibility gap through the presence of its hypostoichiometric phase.

These three models obey the following equations:

$$Model\ \#1 : (1-2y)U^{4+} + yU^{5+} + yNd^{3+}$$
$$Model\ \#2 : (1-\frac{3y}{2})U^{4+} + \frac{y}{2}U^{5+} + yNd^{3+}$$
$$Model\ \#3 : (1-y)U^{4+} + \frac{y}{2}V_O + yNd^{3+}$$

Below y=0.2, the results are in very good agreement with the model #1, suggesting a unique compensation mechanism via the formation of U^{5+} only, and stoichiometric samples, i.e. y=0. This result is perfectly in line with the values reported by Dottavio et al. [10]. Indeed, an overall agreement between reported values and model #1 is observed for y=0.03 and y=0.13. A slight deviation for the

later, meaning a slight amount of oxygen vacancies (i.e. model #3) can be argued. However, if one assume an homogeneous Nd content in both phases instead of two different as described by Dottavio et al. [10], a better agreement with a deviation very close to the XAS result uncertainty is obtained. The absence of measurable hypostoichiometry suggests that the miscibility gap is not observed in our samples up to y=0.2, in contradiction with the previously reported y=0.04 value [10].

An important deviation to the model #1 is clearly visible for the reported sample containing around 10 % of Nd, which is not the case in our measurement. Indeed, Dottavio et al. [10] results led to the presence of about 8 % of oxygen vacancies while our sample demonstrates a pure U^{5+} compensation mechanism. Such reported amount of oxygen vacancies is obtained by considering a different Nd content for each phase. If one assumes again an homogeneous Nd content in both phases, a better agreement is found with a 3 % reduction of the oxygen vacancy content. This remains insufficient to consider their sample in line with sole model #1. But, their sample is out of trends concerning the lattice parameter behavior of the two assumed phases and for the mass fraction of each phase. Thus, even if the observed disagreement is not surprising, it remains unexplained but can be the consequence of sample preparation quality.

The sample around y=0.3 exhibits a substantial deviation from model #1. The presence of detected U^{5+} and U^{6+} valence states demonstrates that both model #1 and #2 are competing in this case. A significant deviation of about 20 % and 10 % for Model #1 and Model #2 respectively is observed. However, the experimental concentration of $[U^{5+}]$ and $[U^{6+}]$ are not sufficient to ensure overall stoichiometry. The presence of oxygen vacancies, i.e. within the Model #3, could compensate the observed deviation, leading to a deduced O/M ratio of 1.97(1), in good agreement with the value reported in [10], and with the possible presence of two phases in our sample.

Finally, the $U_{0.38}Nd_{0.62}O_{2\pm x}$ sample does not agree with any models. The Nd content is out of the natural limits of the Model #1 of y=0.5 and close to the x=0.66 natural limit of Model #2. Due to the possible high uncertainty in U valence evaluation arising from the structural disagreement between references and $U_{0.38}Nd_{0.62}O_{2\pm x}$ sample, it is difficult to draw conclusion about which compensation mechanism is dominating without additional data.

However, 3 different stages can be, at least, extracted from our data. The first region at low Nd content shows U^{5+} formation only, in good agreement with similar results reported in $U_yGd_{1-y}O_2$ for y < 0.14 [28]. Then, formation of oxygen vacancies is observed in addition to oxidation of U^{4+} to higher valence states. But, the presence of a slight amount of U^{6+} is surprising compared to what was already observed for $U_yPu_{1-y}O_{2-x}$ [11] and $U_yCe_{1-y}O_{2-x}$ [12]. At high Nd content, U^{6+} is formed, and O vacancies are also strongly expected.

All of these steps are easily understood when one assume homogeneous repartition of Nd into the UO_2 matrix, and oxygen vacancy affinity for 2 Nd atoms as first neighbors. Indeed, when the concentration of Nd is very low, the probability to find another Nd as first neighbors is low and consequently, the formation of U^{5+} remains the only way to compensate the missing charge, as creating an oxygen vacancy or the formation of U^{6+} are expected to compensate 2 neighboring Nd. Hexavalent uranium U^{6+} is not observed in our case below y=0.2, confirming the fact that U^{6+} formation in fluorite structure is probably energetically too expensive compare to two U^{5+} cations. This is in good agreement with the absence of U^{6+} in the early oxidation stages of UO_2 where U^{4+}/U^{5+} mixture are reported in U_4O_9 and U_3O_7 [30], or in the cases of $U_{1-y}Bi_yO_{2\pm x}$ and $U_{1-y}La_yO_{2\pm x}$ where only U^{5+} formation is reported up to y=0.5 [23] and y=0.4 respectively [31]. These upper limits are two times the value roughly found for Nd doped UO_2, and suggest that the dominating mechanism depends on the dopant nature.

When the Nd concentration increases, the probability to find two Nd as first neighbors increases as well, leading to the competitive compensation mechanisms of forming one V_O, two U^{5+} cations or one U^{6+} cation. Then, when the concentration of Nd is well above y=0.5, U^{5+} are converted to U^{6+}, with a possible formation of V_O, as suggested by comparison to $U_{0.40}Bi_{0.60}O_{1.95}$ [23]. However, both experimental and theoretical assessments are needed, especially in the y= 0.2 ? 0.7 concentration range, to confirm or not these assumptions and give a complete understanding of the charge compensation mechanisms in the $U_{1-y}Nd_yO_{2\pm x}$ system. Moreover, the $U_{1-y}Nd_yO_{2-x}$ and $UU_{1-y}Nd_yO_{2.00}$ phases' formation must be clarified using for example RAMAN spectroscopy and electron microscopies. Indeed, XAS gives only indirect information, and the formation of oxygen vacancies is not necessarily the signature of the formation of these two phases in our samples.

4. Conclusion

Based on U M_4-edge HERFD-XANES analysis, assessment on the charge compensation mechanisms in $U_{1-y}Nd_yO_{2\pm x}$ is reported. When Nd^{3+} cation is substituted into the fluorite lattice, the charge difference is compensate by the formation of U^{5+} cation below approx. y=0.2. This is also observed in $U_{1-y}Gd_yO_2$ in case of similar dopant concentrations [28]. Then, between y=0.2 and approx. 0.6, U^{5+} and U^{6+} cations and oxygen vacancy are competing leading to a hypostoichiometric compound. Finally, the formation of U^{6+} dominates for y > 0.6. Additional experimental points are need in the future to determine accurately the Nd concentration where each mechanism starts.

References

[1] B.J. Lewis, W.T. Thompson, and F.C. Iglesias, 2.20 - Fission Product Chemistry in Oxide Fuels. In Comprehensive Nuclear Materials; Konings, R. J. M., Ed.; Elsevier: Oxford, 2012; Vol. 2, pp 515?546.

[2] D.D. Baron and L. Hallstadius, 2.19 - Fuel Performance of Light Water Reactors (Uranium Oxide and MOX). In Comprehensive Nuclear Materials; Konings, R. J. M., Ed.; Elsevier: Oxford, 2012; Vol. 2, pp 481?514.

[3] H. Kleykamp, *Journal of Nuclear Materials* **131** (1985) 221.

[4] H. Kleykamp, *Journal of Nuclear Materials* **206** (1993) 82.

[5] H.G. Diehl and C. Keller, *Journal of Solid State Chemistry* **3** (1971) 621.

[6] C. Keller and A. Boroujjerdi, *Inorganic Nuclear Chemistry* **34** (1972) 1187.

[7] T. Ohmichi, S. Fukushima, A. Maeda, and H. Watanabe, *Journal of Nuclear Materials* **102** (1996) 40.

[8] L. Desgranges, Y. Pontillon, P. Matheron, M. Marcet, P. Simon, G. Guimbretière, and F. Porcher, *Inorganic Chemistry* **51** (2012) 9147.

[9] G. Dottavio, Y. Pontillon, L. Desgranges, R. Belin, J-C. Richaud, J. Noirot, and C. Valot, *Progress in Nuclear Energy* **72** (2014) 22.

[10] G. Dottavio, Y. Pontillon. L. Desgranges. C. Guéneau, and R. Belin, *Journal of Nuclear Materials* **458** (2015) 394.

[11] C. Guéneau, N. Dupin, B. Sundman, C. Martial, J.-C. Dumas, S. Gossé, S. Chatain, F.D. Bruycker, D. Manara, and R.J.M. Konings, *Journal of Nuclear Materials* **419** (2011) 145.

[12] D.I.R. Norris, and P. Kay, *Journal of Nuclear Materials* **116** (1983) 184.

[13] M.A. Denecke, 19 - X-Ray Spectroscopy in Studies of the Nuclear Fuel Cycle. In X-Ray Absorption and X-Ray Emission Spectroscopy; Bokhoven, J. A. V., Lamberti, C., Eds.; John Wiley & Sons, Ltd, 2016; pp 523?559.

[14] M.R. Antonio and L. Soderholm, Chapter 28 - X-Ray Absorption Spectroscopy of the Actinides. In The Chemistry of the Actinide and Transactinide Elements; Morss, L. R., Edelstein, N. M., Fuger, J., Eds.; Springer Netherlands, 2006; pp 3086-3198.

[15] A. L. Smith, P. Martin, D. Prieur, A.C. Scheinost, P.E. Raison, A.K. Cheetham, and R.J.M. Konings, *Inorganic Chemistry* **55** (2016) 1569.

[16] R. Vauchy, A.-C. Robisson, P.M. Martin, R.C. Belin, L. Aufore, A.C. Scheinost, and F. Hodaj, *Journal of Nuclear Materials* **456** (2015) 115.

[17] R. Vauchy, R.C. Belin, A.-C. Robisson, F. Lebreton, L. Aufore, A.C. Scheinost, and P.M. Martin, *Inorganic Chemistry* **55** (2016) 2123.

[18] D. Prieur, P.M. Baldo, A. Jankowiak, E. Gavilan, A.C. Scheinost, N. Herlet, P. Dehaudt, and P. Blanchart, *Inorganic Chemistry* **50** (2011) 12437.

[19] D. Prieur, P. Martin, F. Lebreton, T. Delahaye, D. Banerjee, A.C. Scheinost, and A. Jankowiak, *Journal of Nuclear Materials* **434** (2013) 7.

[20] J.-F. Vigier, P.M. Martin, L. Martel, D. Prieur, A.C. Scheinost, and J. Somers, *Inorganic Chemistry* **54** (2015) 5358.

[21] F. Lebreton, D. Horlait, R. Caraballo, P.M. Martin, A.C. Scheinost, A. Rossberg, C. Jégou, and T. Delahaye, *Inorganic Chemistry* **54** (2015) 9749.

[22] K. O. Kvashnina, S. M. Butorin, P. Martin, and P. Glatzel, *Physical Review Letters* **111** (2013) 253002.

[23] K. Popa, D. Prieur, D. Manara, M. Naji, J.-F. Vigier, P.M. Martin, O. Dieste Blanco, A.C. Scheinost, T. Prüßmann, T. Vitova, P.E. Raison, J. Somers and R. J. M. Konings *Dalton Transaction* **45** (2016) 7847.

[24] B. Sitaud, P.L. Solari, S. Schlutig, I. Llorens, and H. Hermange, *Journal of Nuclear Materials* **425** (2012) 238.

[25] C. Gauthier, V.A. Solé, R. Signorato, J. Goulon, and E. Moguiline, *Journal of Synchrotron Radiation* **6** (1999) 164.

[26] B. Ravel and M. Newville, *Journal of Synchrotron Radiation* **12** (2005) 537.

[27] A. Rossberg, K.-U. Ulrich, S. Weiss, S. Tsushima, T. Hiemstra, A.C. Scheinost, *Environmental Science and Technology* **43** (2009) 1400.

[28] R. Bès, J. Pakarinen , A. Baena , S. Conradson , M. Verwerft , and F. Tuomisto, *Journal of Nuclear Materials* **489** (2017) 9.

[29] R. Bès, M. Rivenet, P.-L. Solari, K. O. Kvashnina, A.C. Scheinost, and P. M. Martin, *Inorganic Chemistry* **55** (2016) 4260.

[30] G. Leinders, R. Bes, J. Pakarinen, K. Kvashnina, and M. Verwerft, *Inorganic Chemistry* **56** (2017) 6784.

[31] S.M. Butorin, K.O. Kvashnina, D. Prieur, M. Rivenet, and P.M. Martin, *Chemical Communications* **53** (2017) 115.